

Experimental validation of phase space conduits of transition between potential wells

Shane D. Ross,¹ Amir E. BozorgMagham,¹ Shibabrat Naik,^{1,*} and Lawrence N. Virgin²

¹Engineering Mechanics Program, Virginia Tech, Blacksburg, Virginia 24061, USA

²Mechanical Engineering and Materials Science, Duke University, Durham, NC 27708, USA

A phase space boundary between transition and non-transition trajectories, similar to those observed in Hamiltonian systems with rank one saddles, is verified experimentally in a macroscopic system. We present a validation of the phase space flux across rank one saddles connecting adjacent potential wells and confirm the underlying phase space conduits that mediate the transition. Experimental regions of transition are found to agree with the theory to within 1%, suggesting the robustness of phase space conduits of transition in a broad array of two or more degree of freedom experimental systems, despite the presence of small dissipation.

I. INTRODUCTION

Prediction of transition events and the determination of governing criteria has significance in many physical, chemical, and engineering systems where rank-1 saddles are present. To name but a few, ionization of a hydrogen atom under electromagnetic field in atomic physics [1], transport of defects in solid state and semiconductor physics [2], isomerization of clusters [3], reaction rates in chemical physics [4, 5], buckling modes in structural mechanics [6, 7], ship motion and capsize [8–10], escape and recapture of comets and asteroids in celestial mechanics [11–13], and escape into inflation or re-collapse to singularity in cosmology [14]. The theoretical criteria of transition and its agreement with laboratory experiment have been shown for 1 degree of freedom (DOF) systems [15–17]. Detailed experimental validation of the geometrical framework for predicting transition in higher dimensional phase space (≥ 4 , that is for 2 or more DOF systems) is still lacking. The geometric framework of phase space conduits in such systems, termed tube dynamics [11, 12, 18, 19], has not before been demonstrated in a laboratory experiment. It is noted that similar notions of transition were developed for idealized microscopic systems, particularly chemical reactions [1, 20–22] under the names of transition state and reactive island theory. However, investigations of the predicted phase space conduits of transition between wells in multi-well system have stayed within the confines of numerical simulations. In this paper, we present a direct experimental validation of the accuracy of the phase space conduits, as well as the transition fraction obtained as a function of energy, in a 4 dimensional phase space using a controlled laboratory experiment of a macroscopic system.

In [23–25], experimental validation of global characteristics of 1 DOF Hamiltonian dynamics of scalar transport has been accomplished using direct measurement of the Poincaré stroboscopic sections using dye visualization of the fluid flow. In [23, 24], the experimental and computational results of chaotic mixing were

compared by measuring the observed and simulated distribution of particles, thus confirming the theory of chaotic transport in Hamiltonian systems for such systems. Our objective is to validate theoretical predictions of transition between potential wells in an exemplar experimental 2 DOF system, where qualitatively different global dynamics can occur. Our setup consists of a mass rolling on a multi-well surface that is representative of potential energy underlying systems that exhibit transition/escape behavior. The archetypal potential energy surface chosen has implications in transition, escape, and recapture phenomena in many of the aforementioned physical systems. In some of these systems, transition in the conservative case has been understood in terms of trajectories of a given energy crossing a hypersurface or transition state (bounded by a normally hyperbolic invariant manifold of geometry S^{2N-3} in N DOF). In this paper, for $N = 2$, trajectories pass inside a tube-like separatrix, which has the advantage of accommodating the inclusion of non-conservative forces such as stochasticity and damping [7, 10]. The semi-analytical geometry-based approach for identifying transition trajectories has also been considered for periodically forced 2 DOF systems in [26, 27]. Our analytical approach here focuses on identifying separatrices from the unforced dynamics, and generalizes to higher dimensional phase space [5, 28]. Based on the illustrative nature of our laboratory experiment of a 2 DOF mechanical system, and the generality of the framework to higher degrees of freedom [19], we envision the geometric approach demonstrated here can apply to experiments regarding transition across rank-1 saddles in 3 or more DOF systems in many physical contexts.

II. SEPARATRICES IN N DOF

To begin the mathematical description of the invariant manifolds that partition the $2N$ dimensional phase space, we perform a linear transformation of the underlying conservative Hamiltonian. This transformation involves a translation of the saddle equilibrium point to the origin and a linear change of coordinates that uses the eigenvectors of the linear system. The resulting

* Corresponding author: shiba@vt.edu

Hamiltonian near the saddle has the quadratic (normal) form

$$H_2(q_1, p_1, \dots, q_N, p_N) = \lambda q_1 p_1 + \sum_{k=2}^N \frac{\omega_k}{2} (q_k^2 + p_k^2) \quad (1)$$

where N is the number of degrees of freedom, λ is the real eigenvalue corresponding to the saddle coordinates (*reactive coordinates* for chemical reactions) spanned by (q_1, p_1) and ω_k are the frequencies associated with the center coordinates (*bath coordinates* for chemical reactions) spanned by the pair (q_k, p_k) for $k \in 2, \dots, N$.

Next, by fixing the energy level to $h \in \mathbb{R}^+$ and $c \in \mathbb{R}^+$, we can define a co-dimension 1 region $\mathcal{R} \subset \mathbb{R}^{2N}$ in the full phase space by the conditions

$$H_2(q_1, p_2, \dots, q_N, p_N) = h, \quad \text{and} \quad |p_1 - q_1| \leq c. \quad (2)$$

This implies that \mathcal{R} is homeomorphic to the product of a $(2N - 2)$ -sphere and an interval I , that is $\mathcal{R} \cong S^{2N-2} \times I$ where the S^{2N-2} is given by

$$\frac{\lambda}{4} (q_1 + p_1)^2 + \sum_{k=2}^N \frac{\omega_k}{2} (q_k^2 + p_k^2) = h + \frac{\lambda}{4} (p_1 - q_1)^2. \quad (3)$$

This bounding sphere of \mathcal{R} at the middle of the equilibrium region where $p_1 - q_1 = 0$ is defined as follows

$$\mathcal{N}_h^{2N-2} = \left\{ (q, p) \mid \lambda p_1^2 + \sum_{k=2}^N \frac{\omega_k}{2} (q_k^2 + p_k^2) = h \right\}, \quad (4)$$

corresponds to the transition state in chemical reactions (and other systems with similar Hamiltonian structure [7, 10, 11]).

The following phase space structures and their geometry are relevant for understanding transition across the saddle:

a. **NHIM:** The point $q_1 = p_1 = 0$ corresponds to an invariant $(2N - 3)$ -sphere, \mathcal{M}_h^{2N-3} , of periodic and quasi-periodic orbits in \mathcal{R} , and is given by

$$\sum_{k=2}^N \frac{\omega_k}{2} (q_k^2 + p_k^2) = h, \quad q_1 = p_1 = 0. \quad (5)$$

where f is at least of third order. Here, $(q_2, p_2, \dots, q_N, p_N)$ are normal form coordinates and are related to the linearized coordinates via a near-identity transformation. In the neighborhood of the equilibrium point, since the higher order terms in f are negligible compared to the second order terms, the

This is known as the *normally hyperbolic invariant manifold* (NHIM) which has the property that the manifold has a ‘‘saddle-like’’ stability in directions transverse to the manifold and initial conditions on this surface evolve on it for $t \rightarrow \pm\infty$. The role of unstable periodic orbits the 4 dimensional phase space (or more generally, the NHIM in the $2N$ dimensional phase space) in transition between potential wells is acting as anchor for constructing the separatrices of transit and non-transit trajectories.

b. **Separatrix:** The four half open segments on the axes, $q_1 p_1 = 0$, correspond to four high-dimensional cylinders of orbits asymptotic to this invariant S^{2N-3} either as time increases ($p_1 = 0$) or as time decreases ($q_1 = 0$). These are called *asymptotic* orbits and they form the stable and the unstable manifolds of S^{2N-3} . The stable manifolds, $\mathcal{W}_\pm^s(S^{2N-3})$, are given by

$$\sum_{k=2}^N \frac{\omega_k}{2} (q_k^2 + p_k^2) = h, \quad q_1 = 0. \quad (6)$$

where \pm denotes the left and right branches of the stable manifold attached to the NHIM. Similarly, unstable manifolds are constructed and are shown in the saddle space in Fig. 1 as four orbits labeled M. These form the ‘‘spherical cylinders’’ of orbits asymptotic to the invariant $(2N - 3)$ -sphere. Topologically, both invariant manifolds have the structure of $(2N - 2)$ -dimensional ‘‘tubes’’ ($S^{2N-3} \times \mathbb{R}$) inside the $(2N - 1)$ -dimensional energy surface. Thus, they separate two distinct types of motion: transit and non-transit trajectories. While a transition, passing from one region to another, trajectory lies inside the $(2N - 2)$ -dimensional manifold, the non-transition trajectories, bouncing back to their current region of motion, are those outside the manifold.

For a value of the energy just above that of the saddle, the nonlinear motion in the equilibrium region \mathcal{R} is qualitatively the same as the linearized picture above [5, 29, 30]. For example, the NHIM for the nonlinear system which corresponds to the $(2N - 3)$ sphere in (5) for the linearized system is given by

$$\mathcal{M}_h^{2N-3} = \left\{ (q, p) \mid \sum_{k=2}^N \frac{\omega_k}{2} (q_k^2 + p_k^2) + f(q_2, p_2, \dots, q_n, p_n) = h, \quad q_1 = p_1 = 0. \right\} \quad (7)$$

$(2N - 3)$ -sphere for the linear problem is a deformed sphere for the nonlinear problem. Moreover, since the NHIMs persist for higher energies, this deformed sphere \mathcal{M}_h^{2N-3} still has stable and unstable manifolds that are given by

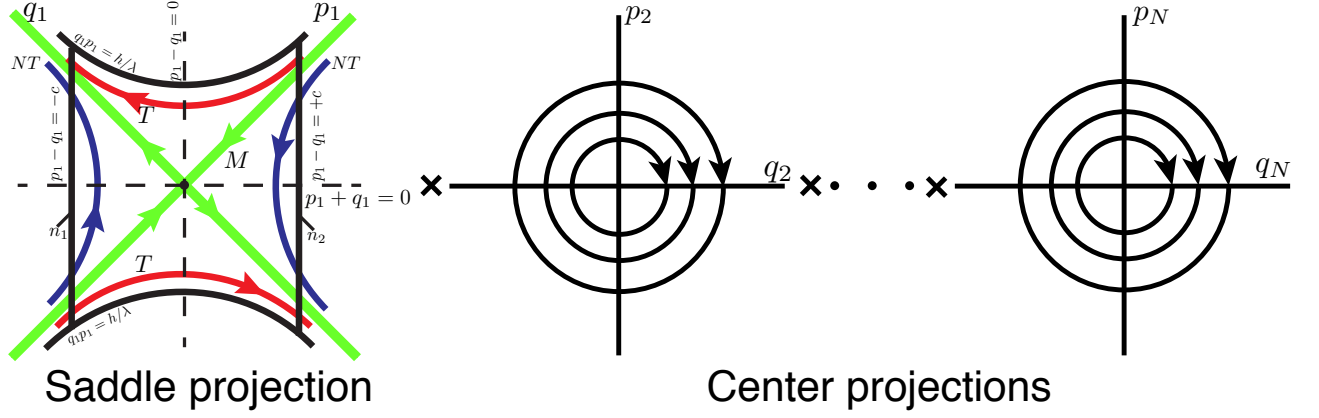


FIG. 1. The flow in the region \mathcal{R} can be separated into saddle \times center $\times \dots \times$ center. On the left, the saddle projection is shown on the (q_1, p_1) -plane. The NHIM (black dot at the origin), the asymptotic orbits on the manifolds (M), two transition trajectories (T), and two non-transition trajectories (NT).

$$\begin{aligned} \mathcal{W}_{\pm}^s(\mathcal{M}_h^{2N-3}) &= \left\{ (q, p) \left| \sum_{k=2}^N \frac{\omega_k}{2} (q_k^2 + p_k^2) + f(q_2, p_2, \dots, q_N, p_N) = h, \quad q_1 = 0. \right. \right\} \\ \mathcal{W}_{\pm}^u(\mathcal{M}_h^{2N-3}) &= \left\{ (q, p) \left| \sum_{k=2}^N \frac{\omega_k}{2} (q_k^2 + p_k^2) + f(q_2, p_2, \dots, q_N, p_N) = h, \quad p_1 = 0. \right. \right\} \end{aligned} \quad (8)$$

This geometric insight is useful for developing numerical methods for *globalization* of the invariant manifolds using numerical continuation [31].

Now, we briefly describe the techniques that can be used to quantify and visualize the high dimensional invariant manifolds. For positive value of excess energy, one can use a normal form computation to obtain higher order terms of (7) and (8). A brief overview of this approach is given in [32] along with applications and results obtained using the computational tool for the Hamiltonian normal form. Another approach is to sample points on these manifolds since the geometry of the manifold is known near the equilibrium point. One would start by taking Poincaré sections and normal form theory that involves high-order expansions around a saddle \times center $\dots \times$ center equilibrium. For example, in 3 DOF, the NHIM has topology S^3 and thus a tube cross-section on a 4D Poincaré section will have topology S^3 for which it is possible to obtain an inside and outside. If $x = \text{constant}$ defines the Poincaré section, then one can project the S^3 structure to two transverse planes, (y, p_y) and (z, p_z) . On each plane, the projection appears as a disk, but because of the S^3 topology, any point in the (z, p_z) projection corresponds to a topological circle in the (y, p_y) (and vice-versa) and from this, one can determine which initial conditions are inside, and thus transit trajectories, as has been performed previously [28, 33].

III. MODEL OF THE 2 DOF EXPERIMENTAL SYSTEM

The initial mathematical model of the transition behavior of a rolling ball on the surface, $H(x, y)$, shown in Fig. 2, is described in [34]. The equations of motion

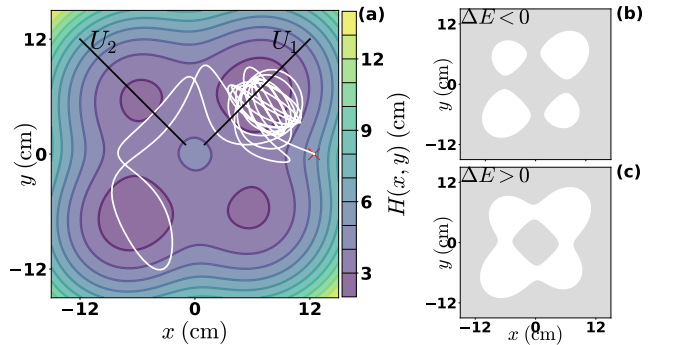


FIG. 2. (a) A typical experimental trajectory, shown in white, on the potential energy surface where the contours denote isoheights of the surface. This instance of the trajectory was traced by the ball released from rest, marked by a red cross. (b) and (c) Show energetically accessible region projected on the configuration space in white for $\Delta E < 0$: $\Delta E = -100$ (cm/s)² and $\Delta E > 0$: $\Delta E = 100$ (cm/s)², respectively.

are obtained from the Hamiltonian, $\mathcal{H}(x, y, p_x, p_y) = T(x, y, p_x, p_y) + V(x, y)$, where mass factors out and where the kinetic energy (translational and rotational for a ball rolling without slipping) is,

$$T = \frac{5}{14} \frac{(1 + H_y^2)p_x^2 + (1 + H_x^2)p_y^2 - 2H_x H_y p_x p_y}{1 + H_x^2 + H_y^2} \quad (1)$$

where $H_{(\cdot)} = \frac{\partial H}{\partial (\cdot)}$. The potential energy is $V(x, y) = gH(x, y)$ where $g = 981 \text{ cm/s}^2$ is the gravitational acceleration and the height function is

$$H = \alpha(x^2 + y^2) - \beta \left(\sqrt{x^2 + \gamma} + \sqrt{y^2 + \gamma} \right) - \zeta xy + H_0. \quad (2)$$

This is the analytical function for the machined surface shown in Fig. 2(b) and the isoheights shown in Fig. 2(c). We use parameter values $(\alpha, \beta, \gamma, \zeta, H_0) = (0.07, 1.017, 15.103, 0.00656, 12.065)$ in the appropriate units [31].

Let $\mathcal{M}(E)$ be the *energy manifold* in the 4D phase space given by setting the total energy equal to a constant, E , i.e., $\mathcal{M}(E) = \{(x, y, p_x, p_y) \in \mathbb{R}^4 \mid \mathcal{H}(x, y, p_x, p_y) = E\}$. The projection of the energy manifold onto the (x, y) configuration space is the region of energetically possible motion for a mass with energy E , and is given by $M(E) = \{(x, y) \mid V(x, y) \leq E\}$. The boundary of $M(E)$ is the zero velocity curve and is defined as the locus of points in the (x, y) plane where the kinetic energy is zero. The mass is only able to move on the side of the curve where the kinetic energy is positive, shown as white regions in Fig. 2(d) and (e). The critical energy for transition, E_c , is the energy of the rank-1 saddle points in each bottleneck, which are all equal. This energy divides the global behavior of the mass into two cases, according to the sign of the excess energy above the saddle, $\Delta E = E - E_c$:

Case 1: $\Delta E < 0$ —the mass is safe against transition and remains inside the starting well since potential wells are not energetically connected (Fig. 2(d)).

Case 2: $\Delta E > 0$ —the mass can transition by crossing the bottlenecks that open up around the saddle points, permitting transition between the potential wells (Fig. 2(e) and Fig. 3(a) show this case).

Thus, transition between wells can occur when $\Delta E > 0$ and this constitutes a necessary condition. The sufficient condition for transition to occur is when a trajectory enters a codimension-1 invariant manifold associated with the unstable periodic orbit in the bottleneck as shown by non-transition and transition trajectories in Fig. 3(a) [18]. In 2 DOF systems, the periodic orbit residing in the bottleneck has an invariant manifold which is codimension-1 in the energy manifold and has topology $\mathbb{R}^1 \times \mathbb{S}^1$, that is a cylinder or tube [31]. This implies that the transverse intersection of these manifolds with Poincaré surfaces-of-sections, U_1 and U_2 , are topologically \mathbb{S}^1 , a closed curve [7, 10, 18]. All the trajectories transitioning to a different potential well (or having just transitioned into the well) are inside a tube manifold, for example as shown in Fig. 3(b) [18, 19]. For every $\Delta E > 0$, the tubes in phase space (or more precisely, within $\mathcal{M}(E)$) that lead to transition are the stable (and that lead to entry are the unstable) manifolds associated with the unstable periodic orbit of energy E . Thus, the mass's imminent transition between adjacent wells can be predicted by considering where it crosses U_1 as shown in Fig. 4, relative to the inter-

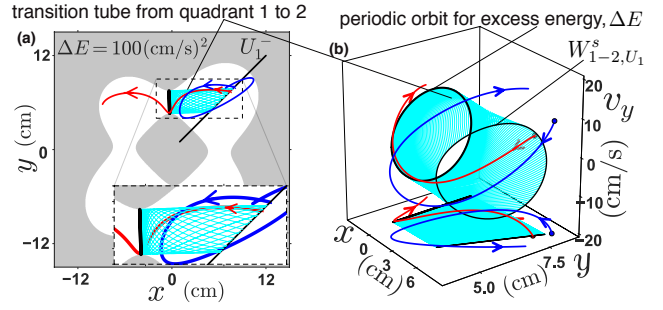


FIG. 3. (a) For a fixed excess energy, ΔE , above the critical value E_c , the permissible regions (in white) are connected by a bottleneck around the saddle equilibria. All motion from the well in quadrant 1 to quadrant 2 must occur through the interior of a stable manifold associated with an unstable periodic orbit in the bottleneck between the quadrants; seen as a 2D configuration space projection of the 3D energy manifold. We show the stable manifold (cyan) and the periodic orbit (black) for an excess energy of $\Delta E = 100 \text{ (cm/s)}^2$. A trajectory crossing the U_1^- section inside the stable manifold will transition (red) into the quadrant 2 well, while one that is outside stays (blue) inside quadrant 1. The zoomed-in inset in the figure shows the structure of the manifold and how precisely the separatrix divides transition and non-transition trajectories. (b) In the (x, y, v_y) projection, the phase space conduit for imminent transition from quadrant 1 to 2 is the stable manifold (cyan) of geometry $\mathbb{R}^1 \times \mathbb{S}^1$ (i.e., a cylinder). The same example trajectories (red and blue) as in (a) that exhibit transition and non-transition behavior starting inside and outside the stable manifold, respectively, are shown in the 3D projection and projected on the (x, y) configuration space. A movie of a nested sequence of these manifolds can be found here.

section of the tube manifold. Furthermore, nested energy manifolds have corresponding nested stable and unstable manifolds that mediate transition. To simplify analysis, we focus only on the transition of trajectories that intersect U_1 in the first quadrant. This surface-of-section is best described in polar coordinates $(r, \theta, p_r, p_\theta)$; $U_1^\pm = \{(r, p_r) \mid \theta = \frac{\pi}{4}, -\text{sign}(p_\theta) = \pm 1\}$, where $+$ and $-$ denote motion to the right and left of the section, respectively [31]. This Hamiltonian flow on U_1^\pm defines a symplectic map with typical features such as KAM tori and chaotic regions, shown in Fig. 4 for two values of excess energy.

Based on these phase space conduits that lead to transition, we would like to calculate what fraction of the energetically permissible trajectories will transition from/into a given well. This can be answered in part by calculating the transition rate of trajectories crossing the rank-1 saddle in the bottleneck connecting the wells. For computing this rate—surface integral of trajectories crossing a bounded surface per unit time—we use the geometry of the tube manifold cross-section on the Poincaré section. For low excess energy, this computation is based on the theory of flux over a rank-1 saddle [35], which corresponds to the action integral around the periodic orbit at energy ΔE . By the Poincaré integral invariant [36], this action is preserved for symplectic maps, such as $P^\pm : U_1^\pm \rightarrow U_1^\pm$, and is equivalent to computing the area of the tube manifold's intersection with the surface-of-section. The transition fraction at each energy, $p_{\text{trans}}(\Delta E)$, is calculated by the fraction of energetically permissible trajectories at a given excess energy, ΔE , that will transition. This is given by

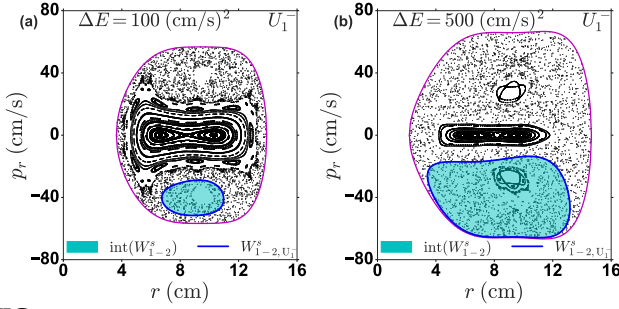


FIG. 4. Poincaré section, $P^- : U_1^- \rightarrow U_1^-$, of trajectories where $U_1^- := \{(r, p_r) | \theta = \pi/4, p_\theta > 0\}$, at excess energy (a) $\Delta E = 100 \text{ (cm/s)}^2$ and (b) $\Delta E = 500 \text{ (cm/s)}^2$. The blue curves with cyan interior denote the intersection of the tube manifold (stable) associated with the unstable periodic orbit with U_1^- . It is to be noted that these manifolds act as a boundary between transition and non-transition trajectories, and may include KAM tori spanning more than one well. The interior of the manifolds, $\text{int}(\cdot)$, denote the region of imminent transition to the quadrant 2 from quadrant 1. A movie showing the Poincaré section for a range of excess energy can be found here.

the ratio of the cross-sections on U_1 of the tube to the energy surface. The transition area, to leading order in ΔE [35], is given by $A_{\text{trans}} = T_{\text{po}} \Delta E$, where $T_{\text{po}} = 2\pi/\omega$ is the period of the periodic orbits of small energy in the bottleneck, where ω is the imaginary part of the complex conjugate pair of eigenvalues resulting from the linearization about the saddle equilibrium point [35]. The area of the energy surface projection on U_1 , to leading order in $\Delta E > 0$, is $A_E = A_0 + \tau \Delta E$, where,

$$A_0 = 2 \int_{r_{\min}}^{r_{\max}} \sqrt{\frac{14}{5} (E_e - gH(r)) (1 + 4H_r^2(r))} dr, \quad (3)$$

$$\text{and } \tau = \int_{r_{\min}}^{r_{\max}} \sqrt{\frac{14}{5} \frac{(1 + 4H_r^2(r))}{(E_e - gH(r))}} dr. \quad (4)$$

The transition fraction, under the well-mixed assumption mentioned earlier, is given in 2 DOF by

$$p_{\text{trans}} = \frac{A_{\text{trans}}}{A_E} = \frac{T_{\text{po}}}{A_0} \Delta E \left(1 - \frac{\tau}{A_0} \Delta E + \mathcal{O}(\Delta E^2) \right). \quad (5)$$

For small positive excess energy, the predicted growth rate is $T_{\text{po}}/A_0 \approx 0.87 \times 10^{-3} \text{ (s/cm)}^2$. For larger values of ΔE , the cross-sectional areas are computed numerically using Green's theorem, see Fig. 6(b).

As with any physical experiment there is dissipation present, but over the time-scale of interest, the motion approximately conserves energy. We compare δE , the typical energy lost during a transition, with the typical excess energy, $\Delta E > 0$, when transitions are possible. The time-scale of interest, t_{trans} , corresponds to the time between crossing U_1 and transitioning across the saddle into a neighboring well. The energy loss over t_{trans} in terms of the measured damping ratio $\zeta \approx 0.025$ is $\delta E \approx \pi \zeta v^2(\Delta E)$ where the squared-velocity $v^2(\Delta E)$ is approximated through the total energy. For our experimental trajectories, all starting at $\Delta E > 1000 \text{ (cm/s)}^2$, we find $\delta E/\Delta E \ll 1$, suggesting the appropriateness of the assumption of short-time conservative dynamics to study transition between wells [7, 10].

IV. EXPERIMENTAL SETUP

We designed a surface (shown in Fig. 2(b)) that has 4 wells, one in each quadrant, with saddles connecting the neighboring quadrants. The surface has 4 stable and 5 saddle (4 rank-1 and 1 rank-2) equilibrium points. Inter-well first order transitions are defined as crossing the rank-1 saddles between the wells. On this high-precision machined surface, accurate to within 0.003 mm and made using stock polycarbonate, a small rubber-coated spherical steel mass released from rest can roll without slipping under the influence of gravity. The mass is released from different locations on the machined surface to generate experimental trajectories. The mass is tracked using a Prosilica GC640 digital camera mounted on a rigid frame attached to the surface as shown in Fig. 2(a), with a pixel resolution of about 0.16 cm. The tracking is done by capturing black

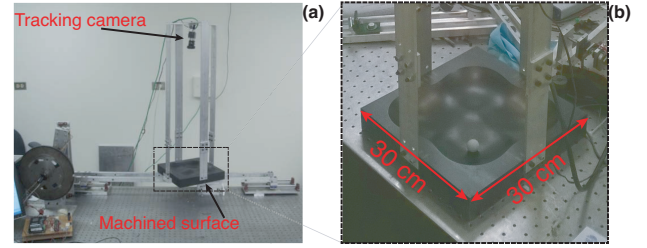


FIG. 5. (a), (b) Experimental apparatus showing the machined surface, tracking camera, and the rubber coated steel ball.

and white images at 50 Hz, and calculating the coordinates of the mass's geometrical center. We recorded 120 experimental trajectories of about 10 seconds long, only using data after waiting at least the Lyapunov time of ≈ 0.4 seconds [34] ensuring that the trajectories were well-mixed in the phase space. To analyze the fraction of trajectories that leave/enter a well, we obtain approximately 4000 intersections with a Poincaré surface-of-section, U_1 , shown as a black line, for the analyzed range of energy. One such trajectory is shown in white in Fig. 2(c). These intersections are then sorted according to energy. The intersection points on U_1 are classified as a transition from quadrant 1 to 2 if the trajectory, followed forward in time, leaves quadrant 1. Four hundred transition events were recorded.

V. RESULTS

For each of the recorded trajectories, we detect intersections with U_1 and determine the instantaneous ΔE . Grouping intersection points by energy, for example Fig. 6(a), we get an experimental transition fraction, Fig. 6(b), by dividing points which transitioned by the total in each energy range. Despite the experimental uncertainty from the image analysis, agreement between observed and predicted values is satisfactory. In fact, a linear fit of the experimental results for small excess energy gives a slope close to that predicted by

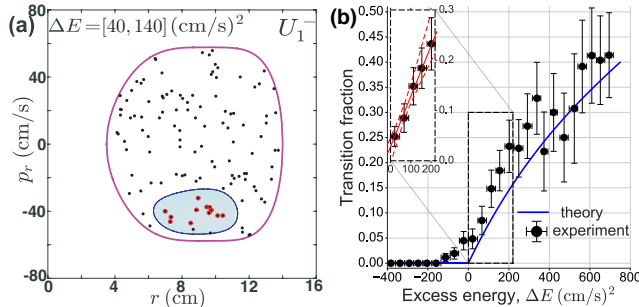


FIG. 6. (a) On the Poincaré section, U_1^- , we show a narrow range of energy ($\Delta E \in (40, 140)$ (cm/s) 2) and label intersecting trajectories as no transition (black) and imminent transition (red) to quadrant 2, based on their measured behavior. The stable invariant manifold associated with the bottleneck periodic orbit at excess energy, $\Delta E = 140$ (cm/s) 2 , intersects the Poincaré section, U_1^- , along the blue curve. Its interior is shown in cyan and includes the experimental transition trajectories. The outer closed curve (magenta) is the intersection of the boundary of the energy surface $\mathcal{M}(\Delta E)$ with U_1^- . (b) Transition fraction of trajectories as a function of excess energy above the saddle. The theoretical result is shown (blue curve) and experimental values are shown as filled circles (black) with error bars. For small excess energy above critical ($\Delta E = 0$), the transition fraction shows linear growth (see inset) with slope $1.0 \pm 0.23 \times 10^{-3}$ (s/cm) 2 and shows agreement with the analytical result (5). A movie of increasing transition area on the Poincaré section, U_1^- , can be found here.

(5) within the margin of error. Furthermore, the clustering of observed transitioning trajectories in each energy range, as in Fig. 6(a), is consistent with the theory of tube dynamics. The predicted transition regions in each energy range account for more than 99% of the

observed transition trajectories.

VI. CONCLUSIONS

We considered a macroscopic 2 DOF experimental system showing transitions between potential wells and a dynamical systems theory of the conduits which mediate those transitions [7, 10, 18]. The experimental validation presented here confirms the robustness of the conduits between multi-stable regions, even in the presence of non-conservative forces, providing a strong footing for predicting transitions in a wide range of physical systems. Given the fragility of other structures to dissipation (for example, KAM tori and periodic orbits), these phase space conduits of transition may be among the most robust features to be found in experiments of autonomous multi-degree of freedom systems. Furthermore, this study lays the groundwork for experimental validation for $N = 3$ or more degrees of freedom system, such as ship dynamics [37], buckling of beams [7] and geodesic lattice domes, hanging roller pins, isomerization and roaming reactions [38, 39].

ACKNOWLEDGMENTS

SDR and LNV thank the NSF for partially funding this work through grants 1537349 and 1537425.

-
- [1] C. Jaffé, D. Farrelly, and T. Uzer, *Phys. Rev. Lett.* **84**, 610 (2000).
- [2] B. Eckhardt, *J. Phys. A-Math. Gen.* **28**, 3469 (1995).
- [3] T. Komatsuzaki and R. S. Berry, *P. Natl. Acad. Sci. USA* **98**, 7666 (2001).
- [4] T. Komatsuzaki and R. S. Berry, *The Journal of Chemical Physics* **110**, 9160 (1999).
- [5] S. Wiggins, L. Wiesenfeld, C. Jaffé, and T. Uzer, *Phys. Rev. Lett.* **86**, 5478 (2001).
- [6] P. Collins, G. S. Ezra, and S. Wiggins, *Phys. Rev. E* **86**, 056218 (2012).
- [7] J. Zhong, L. N. Virgin, and S. D. Ross, *Int. J. Mech. Sci.* **000**, 1 (2018).
- [8] L. N. Virgin, *Dynamics and Stability of Systems* **4**, 56 (1989).
- [9] J. M. T. Thompson and J. R. de Souza, *Proc. R. Soc. Lond. A* **452**, 2527 (1996).
- [10] S. Naik and S. D. Ross, *Commun. Nonlinear Sci.* **47**, 48 (2017).
- [11] C. Jaffé, S. D. Ross, M. W. Lo, J. E. Marsden, D. Farrelly, and T. Uzer, *Physical Review Letters* **89**, 011101 (2002).
- [12] M. Dellnitz, O. Junge, M. W. Lo, J. E. Marsden, K. Padberg, R. Preis, S. D. Ross, and B. Thiere, *Physical Review Letters* **94**, 231102 (2005).
- [13] S. D. Ross, in *Libration Point Orbits and Applications*, edited by G. Gómez, M. W. Lo, and J. J. Masdemont (World Scientific, 2003) pp. 637–652.
- [14] H. P. de Oliveira, A. M. Ozorio de Almeida, I. Damião Soares, and E. V. Tonini, *Phys. Rev. D* **65**, 9 (2002).
- [15] L. N. Virgin and L. A. Cartee, *Int. J. Nonlinear Mech.* **26**, 449 (1991).
- [16] J. A. Gottwald, L. N. Virgin, and E. H. Dowell, *Journal of Sound and Vibration* **187**, 133 (1995).
- [17] J. Novick, M. L. Keeler, J. Giefer, and J. B. Delos, *Phys. Rev. E* **85**, 1 (2012).
- [18] W. S. Koon, M. W. Lo, J. E. Marsden, and S. D. Ross, *Chaos* **10**, 427 (2000).
- [19] F. Gabern, W. S. Koon, J. E. Marsden, S. D. Ross, and T. Yanao, *Few-Body Systems* **38**, 167 (2006).
- [20] A. M. Ozorio de Almeida, N. De Leon, M. A. Mehta, and C. C. Marston, *Physica D: Nonlinear Phenomena* **46**, 265 (1990).
- [21] N. De Leon, M. A. Mehta, and R. Q. Topper, *J. Chem. Phys.* **94**, 8310 (1991).
- [22] C. C. Marston and N. De Leon, *J. Chem. Phys.* **91**, 3392 (1989).
- [23] O. Baskan, M. F. M. Speetjens, G. Metcalfe, and H. J. H. Clercx, *Chaos: An Interdisciplinary Journal of Nonlinear Science* **25**, 103106 (2015).
- [24] O. Baskan, M. F. Speetjens, G. Metcalfe, and H. J. Clercx, *European Journal of Mechanics - B/Fluids* **57**, 1 (2016).
- [25] A. Figueroa, S. Cuevas, and E. Ramos, *Journal of Fluid Mechanics* **815**, 415 (2017).

- [26] E. S. Gawlik, J. E. Marsden, P. C. Du Toit, and S. Campagnola, *Celestial Mechanics and Dynamical Astronomy* **103**, 227 (2009).
- [27] K. Onozaki, H. Yoshimura, and S. D. Ross, *Advances in Space Research* **60**, 2117 (2017).
- [28] F. Gabern, W. S. Koon, J. E. Marsden, and S. D. Ross, *Physica D* **211**, 391 (2005).
- [29] J. Moser, *Comm. Pure Appl. Math.* **11**, 257 (1958).
- [30] H. Waalkens and S. Wiggins, *Regular and Chaotic Dynamics* **15**, 1 (2010).
- [31] See the Supplemental Material for derivation of equations of motion and the computational approach used to obtain the invariant manifolds.
- [32] S. Wiggins, in *IUTAM Symposium on Hamiltonian Dynamics, Vortex Structures, Turbulence*, edited by A. V. Borisov, V. V. Kozlov, I. S. Mamaev, and M. A. Sokolovskiy (Springer Netherlands, Dordrecht, 2008) pp. 189–203; A. D. Burbanks, S. Wiggins, H. Waalkens, and R. Schubert, “Background and documentation of software for computing hamiltonian normal forms,” (2008), software for normal form is available at <https://github.com/Peter-Collins/NormalForm>.
- [33] G. Gómez, W. S. Koon, M. W. Lo, J. E. Marsden, J. Mardmont, and S. D. Ross, *Nonlinearity* **17**, 1571 (2004).
- [34] L. N. Virgin, T. C. Lyman, and R. B. Davis, *Am. J. Phys.* **78**, 250 (2010).
- [35] R. S. MacKay, *Physics Letters A* **145**, 425 (1990).
- [36] J. D. Meiss, *Rev. Mod. Phys.* **64**, 795 (1992).
- [37] L. McCue and A. Troesch, *Ocean Engineering* **32**, 1608 (2005); **33**, 1796 (2006).
- [38] F. A. L. Mauguire, P. Collins, G. S. Ezra, S. C. Farantos, and S. Wiggins, *Theoretical Chemistry Accounts* **133** (2014).
- [39] J. M. Bowman and P. L. Houston, *Chemical Society Reviews* **46**, 7615 (2017).